



# FDM STUDY ON CROSS-DIFFUSIVE EFFECT ON HEAT ABSORBING AND RADIATIVE TRANSIENT HYDROMAGNETIC FLOW OF A NANOFLUID PAST A PROPAGATING UPRIGHT POROUS PLATE

JOSEPH LENGAI SADEMAKI AND EXAVERY PHILEMON ENOCK\*

Email: [jlsademaki@gmail.com](mailto:jlsademaki@gmail.com), [exavery.enock@atc.ac.tz](mailto:exavery.enock@atc.ac.tz)

(Received 7 December 2024; Revision Accepted 20 January 2025)

## ABSTRACT

This investigation delves into the impact of double diffusion on the heat-generating hydro-magnetic transport of water-based nanofluids flowing past a moving permeable plate subjected to heat flux. The nanofluids considered incorporate copper (Cu) and titanium dioxide (TiO<sub>2</sub>) nanoparticles. The study is characterized by the formulation of dimensional quasi-linear partial differential equations (PDEs) with well-defined initial and boundary conditions, which are rendered dimensionless by introducing appropriate non-dimensional parameters. These equations are then resolved numerically using the implicit Crank-Nicolson finite difference scheme implemented in MATLAB. The research meticulously examines the influence of pertinent physical parameters on the velocity profile, temperature distribution, and concentration of reactive species, complemented by graphical illustrations. Furthermore, the study elucidates the impact of these physical variables on the wall shear stress, heat transfer rate, and mass transfer rate, presented in tabular format and subjected to comprehensive analysis. The findings underscore that an increase in the Soret parameter enhances fluid velocity and reactive species concentration, whereas the intensification of the magnetic field and heat flux parameter diminishes fluid velocity. The rate of thermal transfer is observed to escalate with higher values of the heat source, radiation-absorption, and radiative heat flux parameters; conversely, it diminishes with an increase in the Prandtl number. The study reveals superior thermal performance for Cu nanoparticles compared to TiO<sub>2</sub>. A comparative analysis with prior published results substantiates the accuracy of the computational framework, with the outcomes exhibiting exceptional concordance.

**KEYWORDS:** Porous media, Soret number, heat generation, chemical reaction, heat flux.

## INTRODUCTION

Energy scarcity, driven by the finite reserves of natural resources such as coal, oil, and gas, is among the most critical challenges facing the world today [1]. The widening disparity between the rapidly depleting fossil fuel supplies and the escalating energy demands of modern industrialization and contemporary lifestyles necessitates immediate and innovative solutions. Enhancing energy efficiency has emerged as one of the most practical and impactful approaches to mitigating this crisis.

Among heat transfer mediums, water remains the most commonly employed due to its affordability and availability.

Alternative fluids, including lubricants, ethylene glycol, and air, are also utilized but are constrained by their inherently low thermal conductivity [2,3]. Consequently, enhancing the thermal conductivity of heat transfer fluids has been a pivotal area of research for decades. Metals, renowned for their superior thermal conductivity compared to natural fluids, have inspired efforts to augment fluid conductivity by incorporating fine metallic particles. This concept was initially proposed by Maxwell [4]. However, these endeavors faced substantial hurdles, such as sedimentation, machinery corrosion, and pressure drop.

**Joseph Lengai Sademaki**, Department of Applied Science and Social Studies, Arusha Technical College, P.O. Box 296, Arusha, **Tanzania**

**Exavery Philemon Enock** Department of Applied Science and Social Studies, Arusha Technical College, P.O. Box 296, Arusha, **Tanzania**

The advent of nanotechnology in the 21st century revolutionized this domain by enabling the synthesis of nanometer-scale metallic particles, thereby overcoming many earlier limitations. Choi [5] introduced the term nanofluid, building upon Maxwell's foundational theories. Buongiorno et al. [6] conducted experimental investigations, demonstrating that nanofluids exhibit significantly improved thermo-physical properties as heat transfer fluids compared to conventional liquids. Subsequent research by Wang et al. [7] further advanced the understanding of nanofluid behavior and performance. While increasing the volume fraction of nanoparticles enhances the thermal conductivity of nanofluids, exceeding certain thresholds introduces challenges such as elevated viscosity and pressure drops. Thermo-rheological analyses reveal that specific nanoparticle suspensions in base fluids exhibit unique characteristics [8,9]. Metallic nanoparticles, for instance, provide exceptional thermal performance but suffer from stability issues. In contrast, Muneeshwaran et al. [10] highlighted that suspensions of metal oxides in base fluids exhibit greater stability, albeit with relatively lower thermal conductivity. Consequently, studies such as those referenced in [11-15] present compelling insights into the distinct properties and behaviors of metal-based and metal oxide-based nanofluids, enriching the broader understanding of this transformative field.

Radiative thermal propagation and heat generation/absorption are pivotal processes in fluid flow dynamics, particularly in high-temperature regimes where they exert a profound influence on heat transfer mechanisms. These phenomena play a critical role in a broad array of industrial applications, including power generation, aerospace engineering, automotive systems, electronics cooling, and chemical processing. Efficient management of radiative heat transfer and absorption is vital for enhancing the durability, energy efficiency, and operational reliability of such systems. Prasad et al. [16] investigated the effects of thermal and solutal transport in the natural convective reactive magnetohydrodynamic (MHD) flow of nanofluids along a semi-infinite flat plate, accounting for radiative absorption and thermal diffusion. Ali et al. [17] delved into the motion of Newtonian nanofluids, emphasizing radiative attributes, heat source/absorption, mixed convective stagnation-point flow, magnetic field effects, Joule heating, and the influence of chemical reactions on temperature and concentration gradients. Yaseen et al. [18] analyzed heat transfer in both mono and hybrid nanofluids through a Darcy porous medium, considering radiative heat flux and the impact of heat source/absorption in a channel formed by two parallel plates.

Thumma et al. [19] explored the effects of augmented Coriolis forces on nanofluid streams containing cupric oxide and silver nanoparticles, with particular attention to thermal radiation and internal heat sources/sinks. Kodi et al. [20] examined three-dimensional spinning reactive hybrid nanofluid flow over an elongated plate, focusing on internal heat generation under the combined influence of the Hall effect and radiative thermal propagation. Additional insights and findings pertinent to these mechanisms are elaborated upon in references [21-30], offering a comprehensive understanding of their implications across various fluid flow scenarios.

The reviewed body of literature highlights a significant gap in the study of cross-diffusive effects on a radiating magnetohydrodynamic (MHD) water-based nanofluid flowing past an accelerated vertical absorbent plate in the presence of a heat source. This gap underscores the necessity of the present investigation, which aims to examine these effects on a radiating MHD water-based nanofluid containing copper (Cu) or titanium dioxide (TiO<sub>2</sub>) nanoparticles within this specific flow configuration—a domain hitherto unexplored. This research rigorously addresses the phenomenon by deriving the governing equations as quasi-linear partial differential equations (PDEs), complemented by appropriate initial and boundary conditions. These equations are numerically solved using the implicit Crank-Nicolson finite difference method (FDM), a robust computational technique. The study conducts an in-depth analysis of the influence of various dimensionless parameters on flow characteristics, as well as the rates of thermal and solutal transfer. The findings of this study hold substantial practical implications. They contribute to the optimization of heat exchanger design by enhancing heat transfer rates, improving the quality and uniformity of polymer production processes, advancing the performance and reliability of MHD pumps, and ensuring safety and efficiency in nuclear engineering applications.

### Model formulation

Consider a 2D magnetohydrodynamic (MHD) transport involving an unsteady, incompressible, electrically conducting, and diffusive nanofluid that absorbs radiation. This flow occurs near a semi-infinite, vertically accelerating, penetrable plate entrenched in an absorbent medium with a heat source. The coordinate structure is defined by the  $x'$  - axis extending vertically along the flow direction and the  $y'$  - axis oriented perpendicularly to it, as shown in Figure 1. An external magnetic field of uniform strength  $B_0$  is applied analogous to the  $y'$  - axis.

Assuming a negligible magnetic Reynolds number, the induced magnetic and electric fields due to charge polarization are ignored. Additionally, an active homogeneous chemical reaction influences the flow.

The nanofluid is water-based and contains nanoparticles of either copper (Cu) or titanium oxide (TiO<sub>2</sub>). The flow variables depend only on  $y'$  and time  $\tau'$ , given the semi-infinite nature of the plane surface. Fluid properties are treated as constants, except for density variations due to temperature changes.

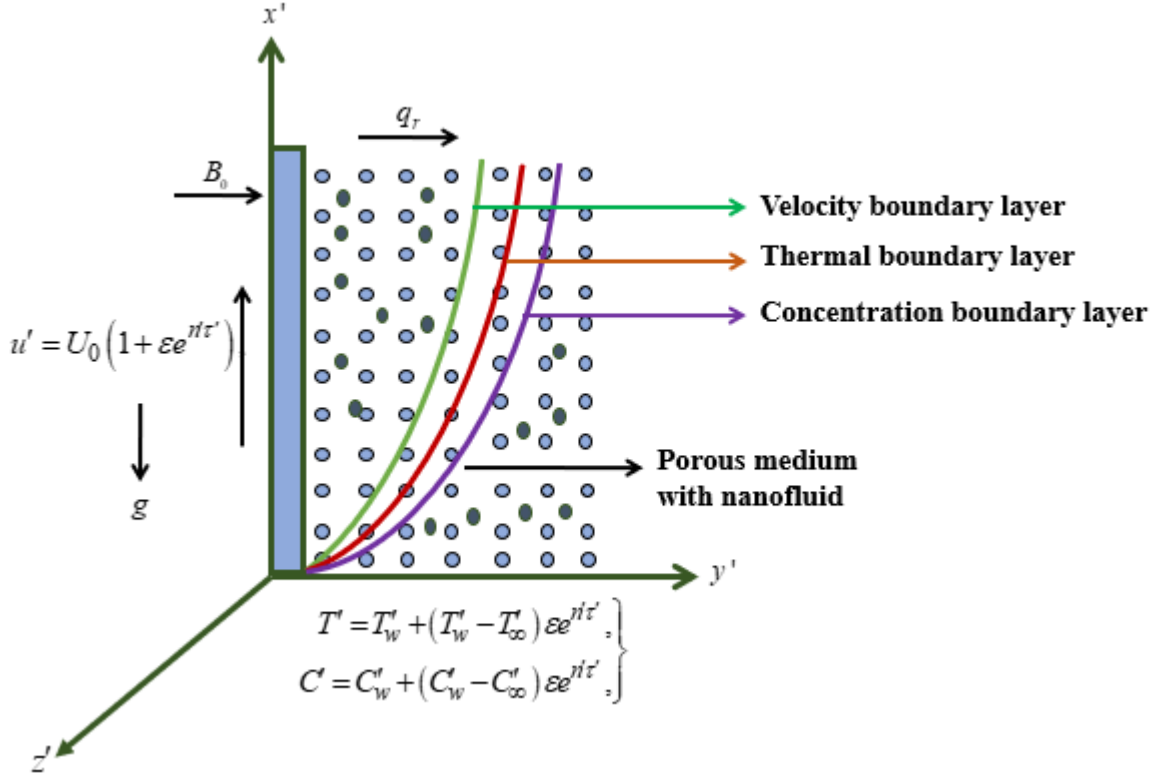


Figure 1. Depicts the physical geometry of the flow

Considering the flow assumptions and employing the Boussinesq approximation, an appropriate mathematical model for the physical problem is formulated as follows (Kodi, 2023):

$$\frac{\partial v'}{\partial y'} = 0 \tag{1}$$

$$\begin{aligned} \rho_{nf} \frac{\partial u'}{\partial \tau'} = & -v' \rho_{nf} \frac{\partial u'}{\partial y'} + \mu_{nf} \frac{\partial^2 u'}{\partial y'^2} + (\rho \beta_{T'})_{nf} (T' - T'_\infty) g - \left( \frac{\mu_{nf}}{k'} + \frac{\sigma B_0^2}{\rho_{nf}} \right) u' \\ & + (\rho \beta_{C'})_{nf} (C' - C'_\infty) - \frac{1}{\rho_{nf}} \frac{\partial p}{\partial x'} \end{aligned} \tag{2}$$

$$\begin{aligned} \frac{\partial T'}{\partial \tau'} = & -v' \frac{\partial T'}{\partial y'} + \alpha_{nf} \frac{\partial^2 T'}{\partial y'^2} - \frac{1}{(\rho c_p)_{nf}} \frac{\partial q'_r}{\partial y'} + Q'_r (C' - C'_\infty) + \frac{D_c K_T}{c_s (\rho c_p)_{nf}} \frac{\partial^2 C'}{\partial y'^2} \\ & + \frac{Q'_s}{(\rho c_p)_{nf}} (T' - T'_\infty) \end{aligned} \tag{3}$$

$$\frac{\partial C'}{\partial \tau'} = -v' \frac{\partial C'}{\partial y'} + D_m \frac{\partial^2 C'}{\partial y'^2} - K_c (C' - C'_\infty) + \frac{D_c K_T}{T_m} \frac{\partial^2 T'}{\partial y'^2} \tag{4}$$

Where  $u'$  and  $v'$  denote components of velocity in  $x'$  and  $y'$  - axis respectively,  $\beta_{T'}$  and  $\beta_{C'}$  are volumetric heat and mass expansion coefficients respectively,  $k'$  represents permeability of the medium,  $g$  denotes gravitational acceleration,  $T'$  and  $C'$  are temperature and concentration components within the boundary layer whereas  $T'_\infty$  and  $C'_\infty$  are the far stream temperature and concentration respectively,  $q'_r$  denotes radiative thermal flux,  $Q'_s$  represents heat source coefficient while  $Q'_r$  is the radiation absorption constant,  $D_m, D_c, K_T$  and  $T_m$  denote mass diffusivity, chemical molecular diffusivity, thermal diffusion, and nanofluid mean temperature coefficients respectively,  $K_c$  is the chemical reaction coefficient, heat capacitance, density, dynamic viscosity, thermal conductivity, and thermal diffusivity of the nanofluid are denoted by  $(\rho c_p)_{nf}, \rho_{nf}, \mu_{nf}, k_{nf}$ , and  $\alpha_{nf}$  respectively which are delineated as follows;

$$\left\{ \begin{array}{l} \rho_{nf} - \varphi \rho_s = (1 - \varphi) \rho_f, \quad (\rho c_p)_{nf} = (1 - \varphi)(\rho c_p)_f + (\rho c_p)_s \varphi, \quad \mu_{nf} = \mu_f (1 - \varphi)^{-2.5}, \\ (\rho \beta)_{nf} = (\rho \beta)_f (1 - \varphi) + (\rho \beta)_s \varphi, \quad k_{nf} = \left( \frac{k_f k_s + 2k_f k_s - 2k_f \varphi (k_f - k_s)}{k_s + 2k_f + 2\varphi (k_f - k_s)} \right), \quad \alpha_{nf} = \left( \frac{k_{nf}}{(\rho c_p)_{nf}} \right) \end{array} \right\}$$

Here,  $\rho_s$  and  $\rho_f$  denote respectively, nanoparticle and water density,  $\varphi$  represents nanoparticle volume fraction,  $k_f$  and  $k_s$  are thermal conductivities of water and nanoparticles respectively,  $\mu_f$  denotes dynamic viscosity of water.

In view of a model for an optically thin medium, an appropriate representation for the radiative heat flux in agreement with Cramer and Pai (1973) is given by

$$\frac{\partial q'_r}{\partial y'} = 4(T' - T'_\infty)I, \quad (5)$$

Here;  $I = \int_0^\infty K_\lambda (\partial_{eb\lambda} / \partial T') d\lambda$ , where  $K_\lambda$  represents the absorption coefficient along the wall,  $eb\lambda$  denotes

Planck's function.

The appropriate governing initial and boundary conditions for the velocity, temperature, and concentration profiles for the physical problem are provided by

$$\left\{ \begin{array}{l} u'(y', \tau') = 0, T' = T'_\infty, C' = C'_\infty \quad \forall y' \text{ and } \tau' \leq 0 \\ \left. \begin{array}{l} u' = U_0 (1 + \varepsilon e^{n'\tau'}), \quad T' = T'_w + (T'_w - T'_\infty) \varepsilon e^{n'\tau'}, \\ C' = C'_w + (C'_w - C'_\infty) \varepsilon e^{n'\tau'}, \end{array} \right\} \left. \begin{array}{l} T' = T'_w + (T'_w - T'_\infty) \varepsilon e^{n'\tau'}, \\ C' = C'_w + (C'_w - C'_\infty) \varepsilon e^{n'\tau'}, \end{array} \right\} \text{ at } y' = 0 \text{ for } \tau' > 0 \\ u'(y', \tau') = 0, T' \rightarrow T'_\infty, C' \rightarrow C'_\infty \quad \text{as } y' \rightarrow \infty \text{ for } \tau' > 0 \end{array} \right\} \quad (6)$$

From the continuity equation,  $v'$  is constant, therefore we can assume normal velocity along the plate is a non-negative constant  $v_0$ , which is the scale for suction. The parameter  $\varepsilon$  is taken to be less than unity.

In consideration of the region outside the boundary layer, Eq. (2) yields

$$-\frac{1}{\rho_{nf}} \frac{\partial p}{\partial x'} = \frac{\partial U_{\infty}}{\partial \tau'} + \left( \frac{\nu_f}{k'} + \frac{\sigma B_0^2}{\rho_{nf}} \right) U'_{\infty}. \quad (7)$$

Consider the following dimensionless variables;

$$\begin{aligned} u &= \frac{u'}{U_0}, \quad v = \frac{v'}{v_0}, \quad \xi = \frac{v_0 y'}{\nu_f}, \quad U_{\infty} = \frac{U'_{\infty}}{U_0}, \quad \text{Pr} = \frac{(\mu c_p)_f}{k_f}, \quad U_p = \frac{U'_p}{U_0}, \quad t = \frac{\tau' v_0^2}{\nu_f}, \\ C &= \frac{(C' - C'_{\infty})}{(C'_w - C'_{\infty})}, \quad Sc = \frac{\nu_f}{D_m}, \quad \theta = \frac{(T' - T'_{\infty})}{(T'_w - T'_{\infty})}, \quad n = \frac{n' \nu_f}{v_0^2}, \quad K_p = \frac{k' v_0^2}{\nu_f^2}, \quad M = \frac{\sigma B_0^2 \nu_f}{\rho_f v_0^2}, \\ H_S &= \frac{Q'_s \nu_f}{(\rho c_p)_f v_0^2}, \quad K_r = \frac{\nu_f K_c}{v_0^2}, \quad N = \frac{4I \nu_f}{(\rho c_p)_f v_0^2}, \quad Du = \frac{D_c K_T (C'_w - C'_{\infty})}{\nu_f c_s c_p (T'_w - T'_{\infty})}, \\ Sr &= \frac{D_c K_T (C'_w - C'_{\infty})}{\nu_f T_m (T'_w - T'_{\infty})}, \quad Gr = \frac{\nu_f g (\rho \beta_{T'})_f (T'_w - T'_{\infty})}{U_0 v_0^2}, \quad R = \frac{Q'_r (C'_w - C'_{\infty})}{v_0^2 (T'_w - T'_{\infty})}, \\ Gc &= \frac{\nu_f g (\rho \beta_{C'})_f (C'_w - C'_{\infty})}{U_0 v_0^2}, \quad S = \frac{\nu_0}{U_0}. \end{aligned}$$

Here,  $\text{Pr}$  is Prandtl number,  $Sc$  is Schmidt number,  $Du$  is Dufour number,  $Sr$  is Soret number,  $Gr$  is thermal Grashof number,  $Grm$  is mass Grashof number,  $\nu_f$  is kinematic viscosity of the fluid. Introducing the dimensionless variables described in the system of underlying partial differential equations for the physical problem, we obtain a dimensionless model as follows;

$$a_1 \left( \frac{\partial u}{\partial t} - S \frac{\partial u}{\partial \xi} \right) = \frac{dU_{\infty}}{dt} + a_2 \frac{\partial^2 u}{\partial \xi^2} + a_3 (Gr\theta + GcC) + \left( M + \frac{1}{K_p} \right) (U_{\infty} - u) \quad (8)$$

$$b_1 \left( \frac{\partial \theta}{\partial t} - S \frac{\partial \theta}{\partial \xi} - RC \right) = b_2 \frac{\partial^2 \theta}{\partial \xi^2} - \frac{(N - H_S)}{\text{Pr}} \theta + \frac{Du}{\text{Pr}} \frac{\partial^2 C}{\partial \xi^2} \quad (9)$$

$$\frac{\partial C}{\partial t} = S \frac{\partial C}{\partial \xi} + \left( \frac{1}{Sc} \right) \frac{\partial^2 C}{\partial \xi^2} + Sr \frac{\partial^2 \theta}{\partial \xi^2} - KrC \quad (10)$$

The conforming initial and boundary settings are given as;

$$\left\{ \begin{array}{l} t < 0; u = 0, \theta = 0, C = 0, \quad \text{for all } \xi \\ t \geq 0; u = U_p, \theta = 1 + \varepsilon e^{n\tau}, C = 1 + \varepsilon e^{n\tau}, \quad \text{at } \xi = 0 \\ u \rightarrow U_{\infty} = 1 + \varepsilon e^{n\tau}, \theta \rightarrow 0, C \rightarrow 0, \quad \text{as } \xi \rightarrow \infty \end{array} \right\} \quad (11)$$

Additional parameters depicted in the dimensionless model are expressed as follows;

$$\left\{ \begin{array}{l} a_1 = (1-\varphi) + \varphi \left( \frac{\rho_s}{\rho_f} \right), a_2 = (1-\varphi)^{-2.5}, a_3 = \left[ (1-\varphi) + \varphi \left( \frac{(\rho\beta)_s}{(\rho\beta)_f} \right) \right], \\ b_1 = \left[ (1-\varphi) + \varphi \left( \frac{(\rho c_p)_s}{(\rho c_p)_f} \right) \right], b_2 = \frac{(1+2\varphi) + (2-2\varphi)(k_f/k_s)}{(1-2\varphi) + (2+2\varphi)(k_f/k_s)}. \end{array} \right\}$$

**Table 1.** Thermo-physical properties of nanoparticles and base fluid [46].

Properties	water	Copper	Titanium Oxide
$C_p (J / KgK)$	4179	385	686.2
$\rho (Kg / m^3)$	997.1	8933	4250
$k (w / mK)$	0.613	400	8.9538
$\beta 10^{-5} (1/K)$	21	1.67	0.9

The shear stress, rate of thermal, and solutal propagation in the form of Nusselt and Sherwood numbers are expressed as follows:

$$S_f = \left( \frac{\partial u}{\partial \xi} \right)_{\xi=0}, Nu = - \left( \frac{\partial \theta}{\partial \xi} \right)_{\xi=0} \text{ and } Sh = - \left( \frac{\partial C}{\partial \xi} \right)_{\xi=0} \quad (12)$$

### Computational flow

The coupled quasi-linear PDEs (8) – (10) collectively with initial and boundary regulations Eqs. (11) represents the flow determining equations of the proposed model. The analytical (exact) solutions to mentioned equations are practically almost not possible. Thus, the implicit Crank-Nicolson finite difference scheme is prescribed to solve Eqs. (8) – (10) along with Eqs. (11) The forward time central in space for  $u$ ,  $\theta$  and  $C$  is given as follows:

$$a_1 \left[ \frac{u_j^{n+1} - u_j^n}{\Delta t} - S \left( \frac{u_{j+1} - u_{j-1}}{2\Delta\xi} \right) \right] = \frac{dU_\infty}{dt} + a_2 \left( \frac{u_{j+1} - 2u_j + u_{j-1}}{(\Delta\xi)^2} \right) + a_3 \left( Gr\theta_j^{n+1} + GcC_j^{n+1} \right) + \left( M + \frac{1}{K_p} \right) (U_\infty - u_j^{n+1}) \quad (13)$$

$$b_1 \left[ \frac{\theta_j^{n+1} - \theta_j^n}{\Delta t} - S \left( \frac{u_{j+1} - u_{j-1}}{2\Delta\xi} \right) - R\phi_j^{n+1} \right] = b_2 \left( \frac{\theta_{j+1} - 2\theta_j + \theta_{j-1}}{(\Delta\xi)^2} \right) - \frac{(N - H_S)}{Pr} \theta_j^{n+1} + \frac{Du}{Pr} \left( \frac{C_{j+1} - 2C_j + C_{j-1}}{(\Delta\xi)^2} \right) \quad (14)$$

$$\frac{C_j^{n+1} - C_j^n}{\Delta t} = S \left( \frac{C_{j+1} - C_{j-1}}{2\Delta\xi} \right) + \left( \frac{1}{Sc} \right) \left( \frac{C_{j+1} - 2C_j + C_{j-1}}{(\Delta\xi)^2} \right) + Sr \left( \frac{\theta_{j+1} - 2\theta_j + \theta_{j-1}}{(\Delta\xi)^2} \right) - Kr C_j^{n+1} \quad (15)$$

The transformed initial and boundary conditions are given as follows;

$$\left. \begin{aligned} & \left\{ \begin{aligned} & u_j^0 = 0, \theta_j^0 = 0, C_j^0 = 0 \quad \forall j \\ & u_0^{n+1} = U_p, \theta_0^{n+1} = 1 + \varepsilon e^{n\tau}, C_0^{n+1} = 1 + \varepsilon e^{n\tau} \quad \text{at } \xi=0 \\ & u_j^{n+1} \rightarrow U_\infty = 1 + \varepsilon e^{n\tau}, \theta_j^{n+1} \rightarrow 0, C_j^{n+1} \rightarrow 0, \quad \text{as } j \rightarrow j_{\max} \end{aligned} \right\} \end{aligned} \right\} \quad (16)$$

Here, index  $i$  characterizes the space  $y$ ,  $\Delta\xi$  signify mesh in  $y$  – direction; index  $j$  characterizes the temporal  $t$ , and  $\Delta t$  represents the mesh in  $\tau$  – direction. Thus, the values of flow variables such as  $u$ ,  $C$ , and  $\theta$  at grid point  $t = 0$  are identified; hence, the velocity field, concentration field, and thermal field have been solved at a time  $t_{j+1} = t_j + \Delta t$  employing the known values of the earlier time  $t = t_j$  for all  $j = 0, 1, 2, \dots, N - 1$ . These processes are recurrent until the desired solution of the flow fields converges. The mesh size is fixed at  $\Delta t = 0.0125$  and  $\Delta\xi = 0.025$  for the whole computational process to ensure stability and convergence. The numerical code is validated and accurate by comparing it.

**Code validation**

Table 2 validates the computational results with Prasad et al. [16] under similar conditions. With some parameters set to zero, a similar flow model is obtained for appropriate comparison of results. As seen in the table, the presented results of the Nusselt number give an equivalent outcome to the existing ones; thus, they confirm and validate all the outcomes of this present analysis.

**Table 2:** Comparison of the Nusselt number when  $H_s = 0, S = 0.1$  and  $\varphi = 0.15$ .

$Du$	$R$	$N$	Prasad et al [16]		Present work	
			$Nu$ for $Cu - H_2O$	$Nu$ for $TiO_2 - H_2O$	$Nu$ for $Cu - H_2O$	$Nu$ for $TiO_2 - H_2O$
0.1			0.9221	0.9555	0.92211	0.95550
0.2			0.8898	0.9270	0.88980	0.92701
0.3			0.8574	0.8986	0.85742	0.89860
	2		0.4558	0.5502	0.45580	0.55022
	4		0.8920	0.6157	0.89201	0.61571
	6		2.2399	1.7815	2.23990	1.78150
		3	0.9468	1.4675	0.94683	1.46754
		4	1.4974	1.9287	1.49742	1.92873
		5	2.4122	2.3096	2.41221	2.30961

**DISCUSSION OF RESULTS**

To gain a deeper understanding of the problem, numerical computations for the dimensionless flow profiles and engineering quantities was computed utilizing relevant parameter values for two distinct water-based nanofluids. Specifically, dual solutions for  $TiO_2-H_2O$  and  $Cu-H_2O$  nanofluids was examined and presented. To validate the accuracy and reliability of the results, a comparison of computed engineering quantities with the findings of Prasad et al. [16] was done for various parameter configurations. These comparisons, summarized in Table 2, exhibit remarkable concordance, further affirming the exceptional precision and robustness of our current outcomes.

Figures 2 and 3 illustrate the influence of the Soret number ( $Sr$ ) on the velocity and concentration trends, correspondingly.

It is evident that an increase in  $Sr$  enhances both the velocity and concentration boundary layers. This can be explained by the Soret effect, where a mass flux is generated due to the thermal gradient resulting from a concentration disparity among species. A similar outcome was observed by Sulochana et al. [21]. Figures 4 and 5 portray the stimulus of radiation absorption on the velocity and temperature variations, respectively. It is manifest from these graphs that increasing the radiation absorption effect tends to enhance both velocity and temperature within the stream. When radiation absorption increases, more thermal energy is absorbed by the fluid, leading to an escalation in the fluid's temperature. This elevated temperature reduces the fluid's density in regions where the absorption is high, thereby generating buoyancy forces that drive the fluid movement.

Figures 6 and 7 illustrate the behavior of the velocity and temperature fields in reaction to an increasing radiative heat flux. As heat flux increases, the fluid's internal thermal energy reduces. As the temperature of the fluid decreases due to this energy loss, the buoyancy forces that drive fluid motion are also weakened. This reduction in buoyancy results in lower fluid velocity. Therefore, the collective effect of reduced thermal energy and diminished buoyancy forces leads to a diminution in both temperature and velocity profiles. Figure 8 demonstrates the influence of the magnetic field strength on the pace of Cu- H<sub>2</sub>O and TiO<sub>2</sub>- H<sub>2</sub>O nanofluids. As the magnetic strength evolves, the velocity curve of both nanofluids diminishes. This reduction is due to the incorporation of a crosswise magnetic field, which generates a retarding Lorentz force in the electrically conducting fluid. This force impedes fluid motion within the boundary layer, thereby decreasing velocity. A similar result was reported by Prasad et al. [16]. It's visible in Figure 9 that the velocity profile upsurges with an increment in porosity. This trend is familiar since drag within the flow regime reduces as the pores get larger. Figures 10 and 11 exemplify the outcome of the heat generation on the velocity and temperature profile. Similar to the effects observed with the radiation parameter, an enhancement of the heat source parameter lessens the heat frontier layer thickness and boosts the heat transfer rate, consistent with the underlying physical principles. Figures 12 and 13 highlight that a surge in both the thermal Grashof number ( $Gr$ ) and the solutal Grashof number ( $Gc$ ) results in an enhancement in velocity within the Cu-

H<sub>2</sub>O and TiO<sub>2</sub>- H<sub>2</sub>O nanofluids. This observation suggests that the current study involves buoyancy-assisted flow, driven by both thermal and mass buoyancy forces. This finding aligns with the fallouts testified by Sulochana et al. [21]. Figures 14 and 15 highlight the impact of the Dufour number on both the temperature and velocity fields. The figures demonstrate that an enhanced Dufour effect intensifies the temperature field and both velocity fields. The Dufour term appears in the energy equation due to the conversion of concentration gradients into thermal energy variations within the flow regime. This phenomenon is crucial for augmenting the velocity field and is effective in increasing thermal energy, thereby elevating the temperature field. Consequently, both primary and secondary velocities accelerate. The influence of the Prandtl number on the temperature profile produced the anticipated outcome. Specifically, as shown in Figure 16, the heat and solute frontier layer thickness declines with higher Prandtl number values. This finding is unswerving with the results reported by Raghunath et al. [46]. With reference to Figure 17, the concentration profile deteriorates with the upsurge in Schmidt number ( $Sc$ ). The trend is a physical reality since it indicates that the mass diffusivity is relatively low compared to the kinematic viscosity. Figure 18 illustrates the upshot of the chemical reaction on concentration curves. The figure clearly shows that an increase in the chemical reaction parameter leads to a reduction in the concentration profile within the flow. This behavior aligns with the general physical principle that a higher chemical reaction parameter results in a diminished concentration due to the increased rate of chemical reactions.

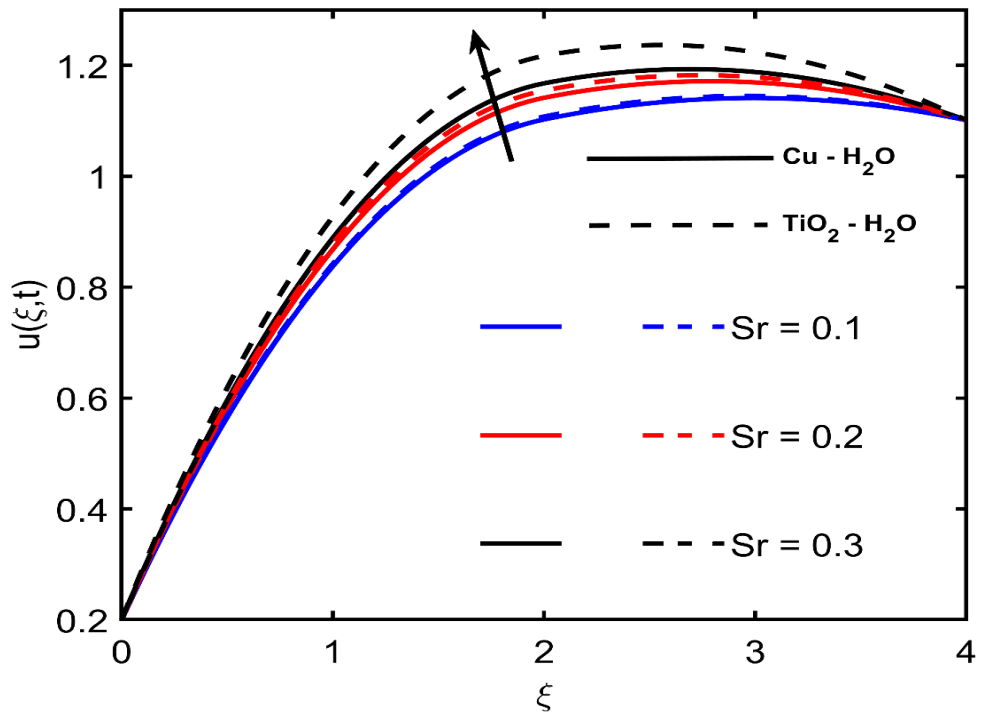


Fig.2: Velocity profiles  $u$  versus  $Sr$ .

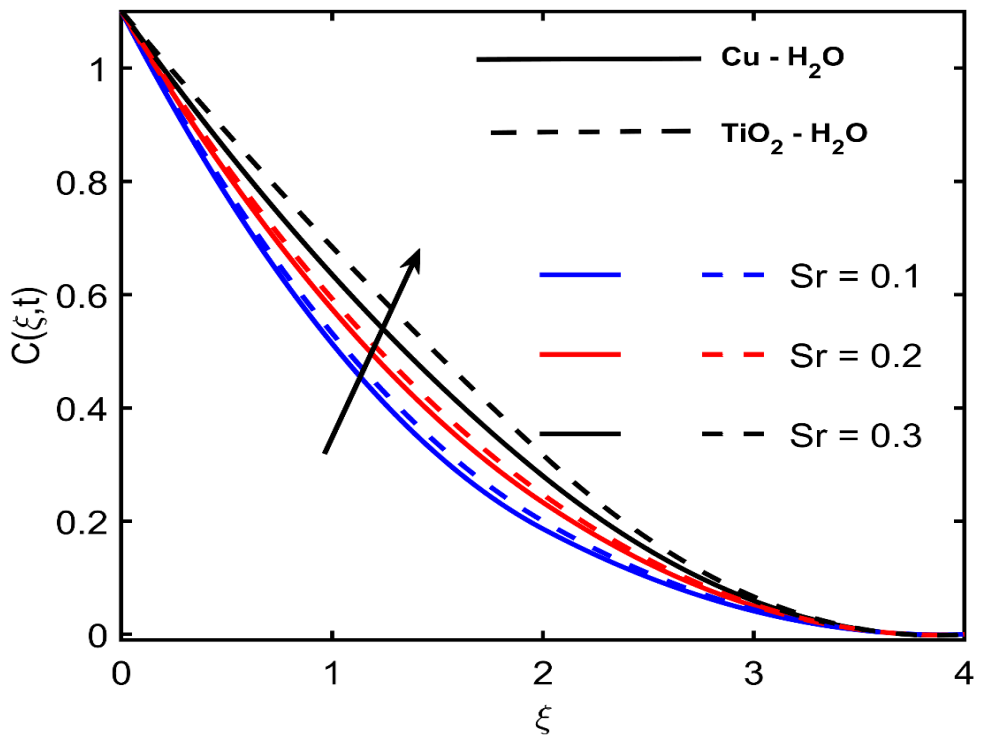


Fig.3: Concentration profiles  $C$  versus  $Sr$ .

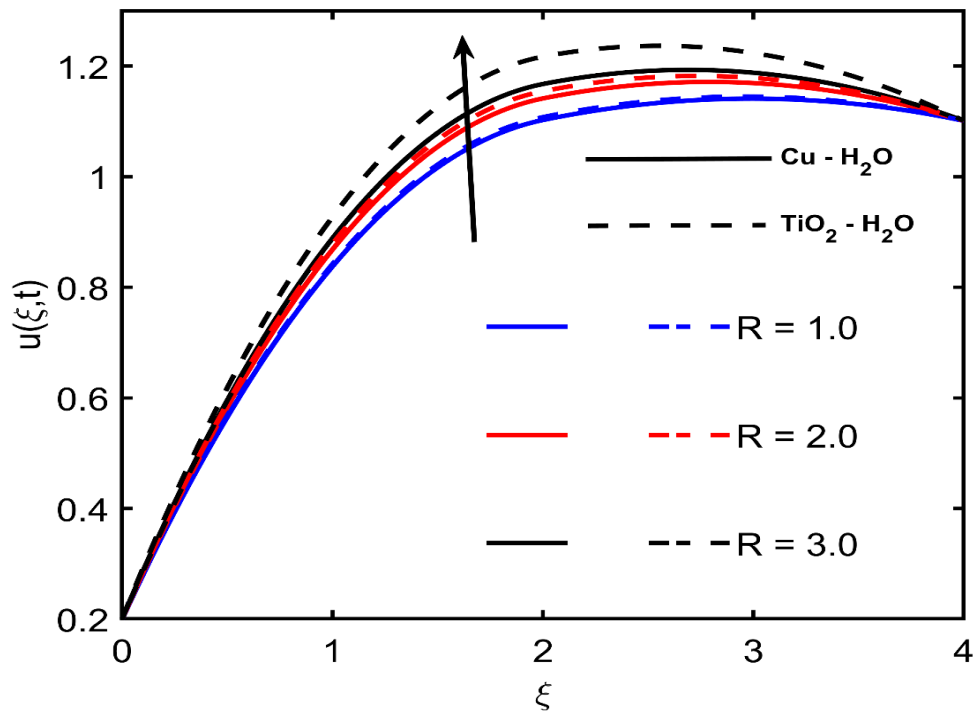


Fig.4: Velocity profiles  $u$  versus  $R$ .

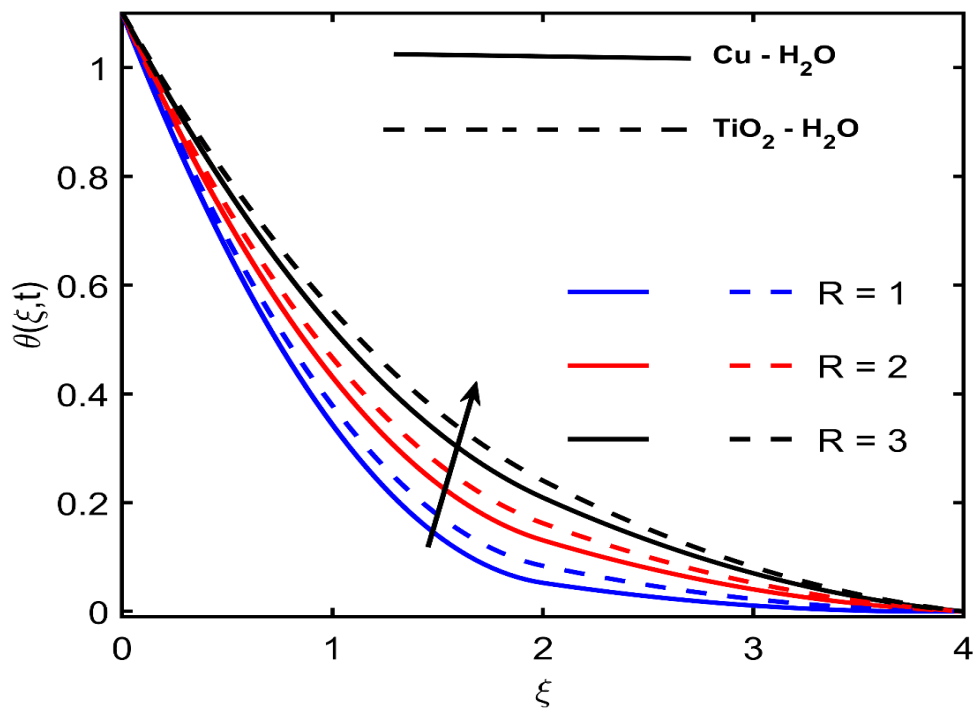


Fig.5: Temperature profiles  $\theta$  versus  $R$ .

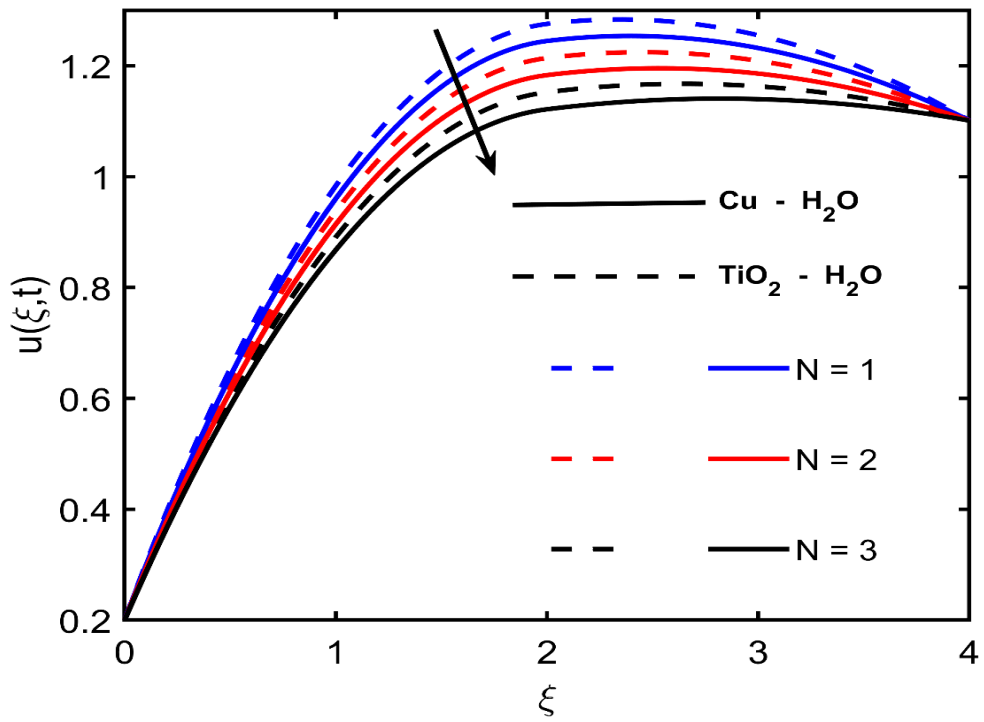


Fig.6: Velocity profiles  $u$  versus  $N$ .

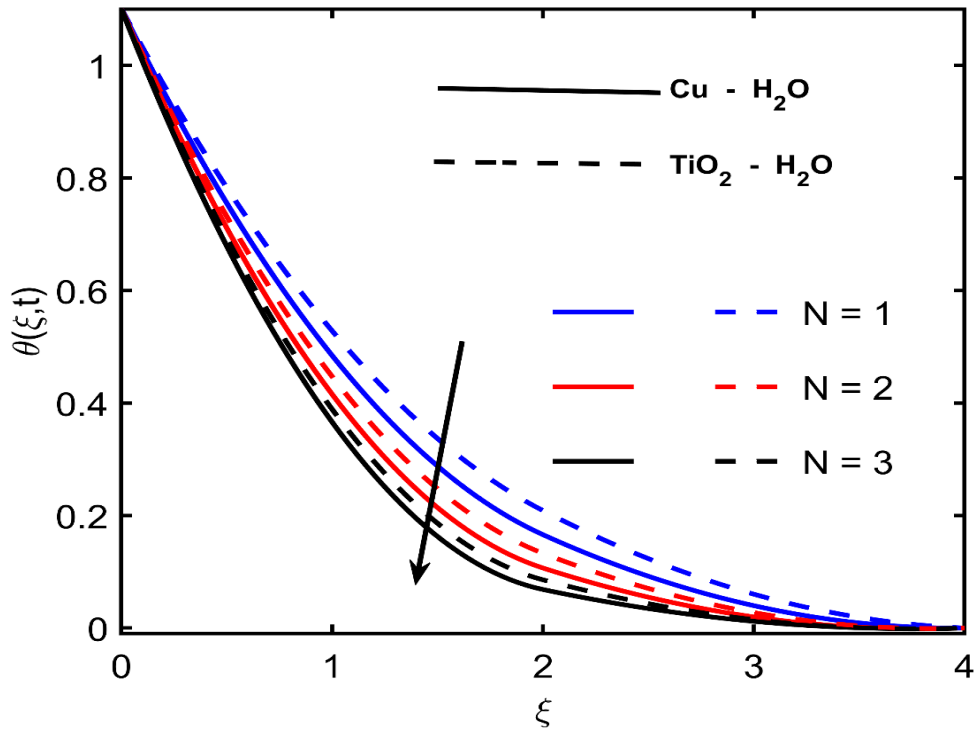


Fig.7: Temperature profiles  $\theta$  versus  $N$ .

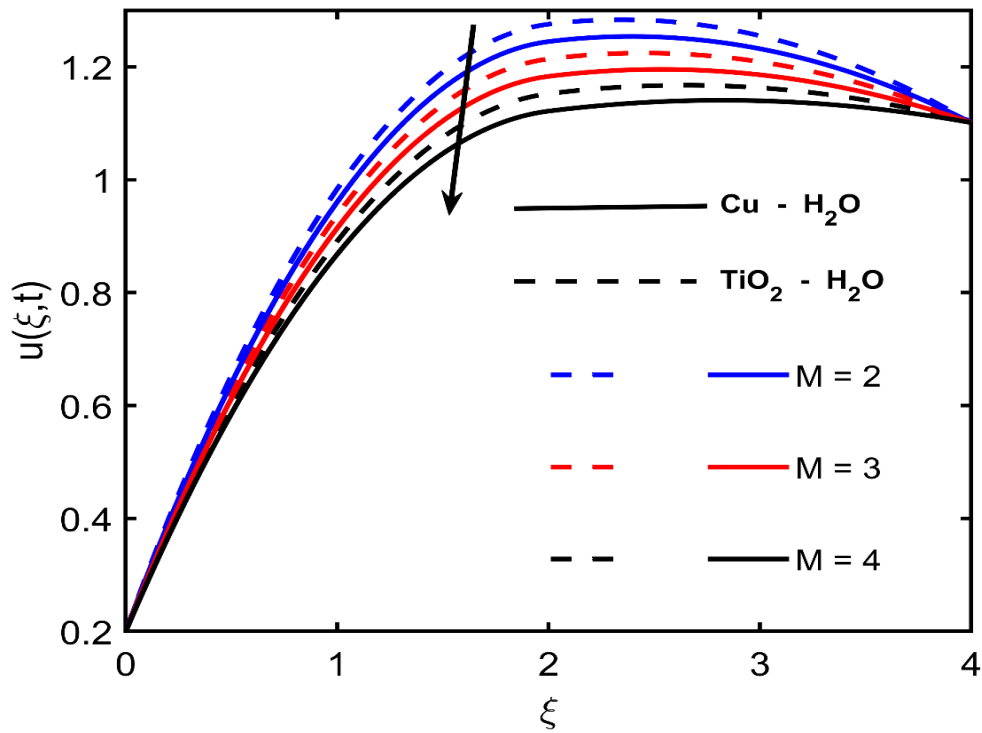


Fig.8: Velocity profiles  $u$  versus  $M$ .

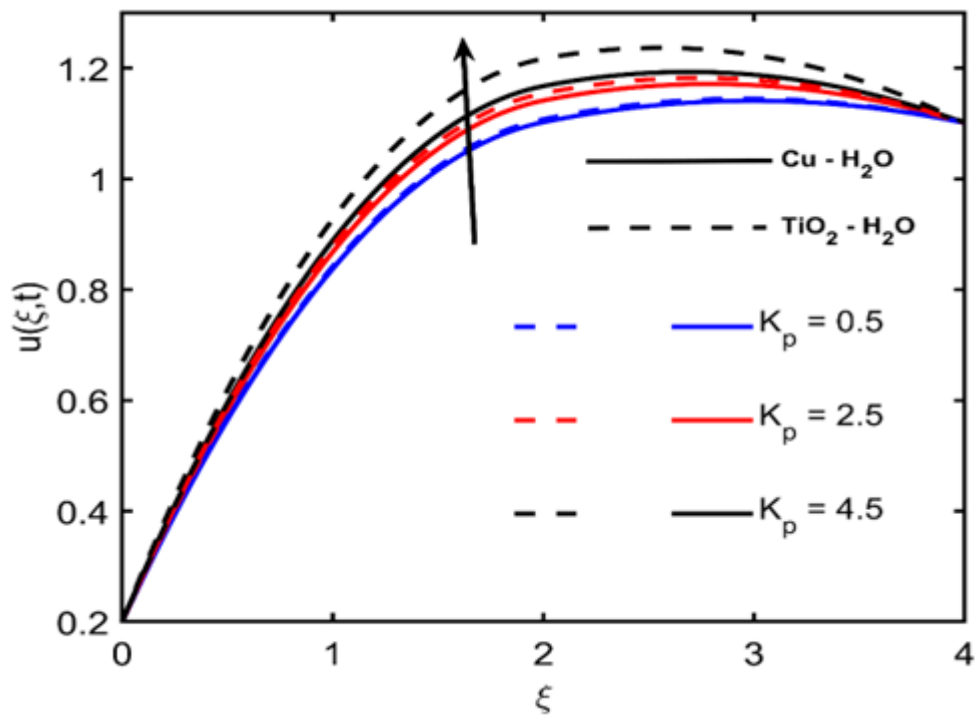


Fig.9: Velocity profiles  $u$  versus  $K_p$ .

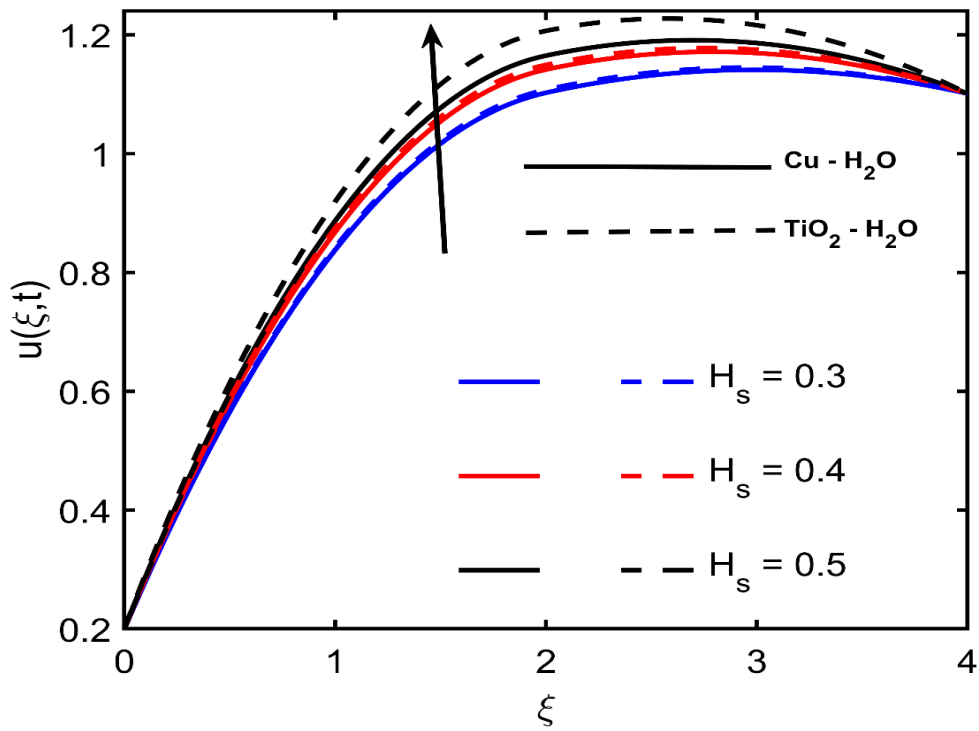


Fig.10: Velocity profiles  $u$  versus  $H_s$ .

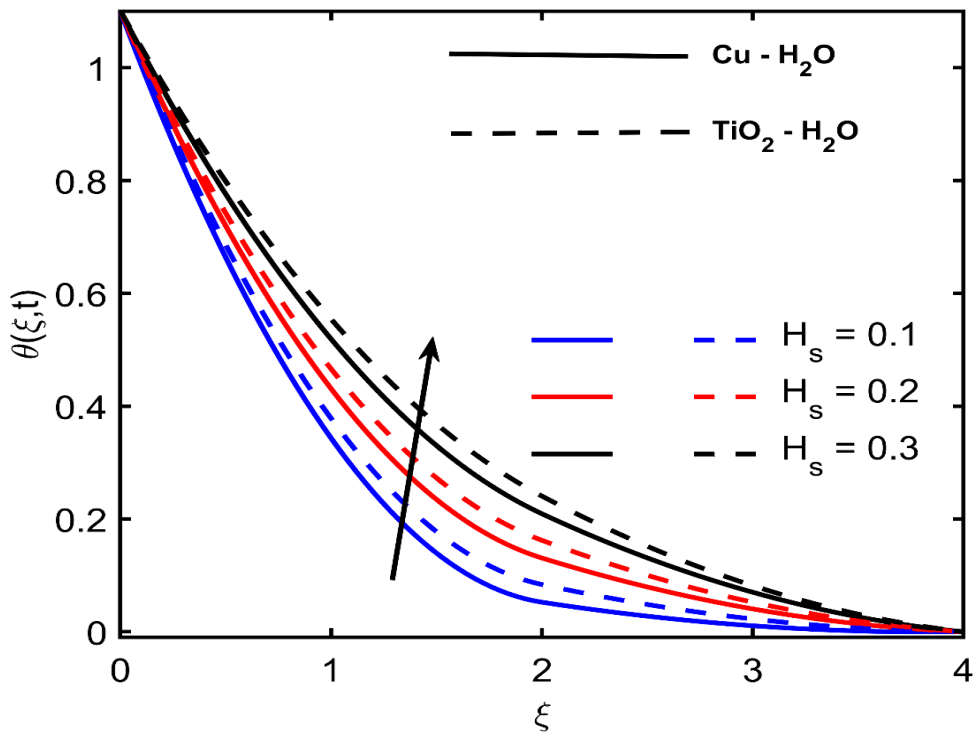


Fig.11: Temperature profiles  $\theta$  versus  $H_s$ .

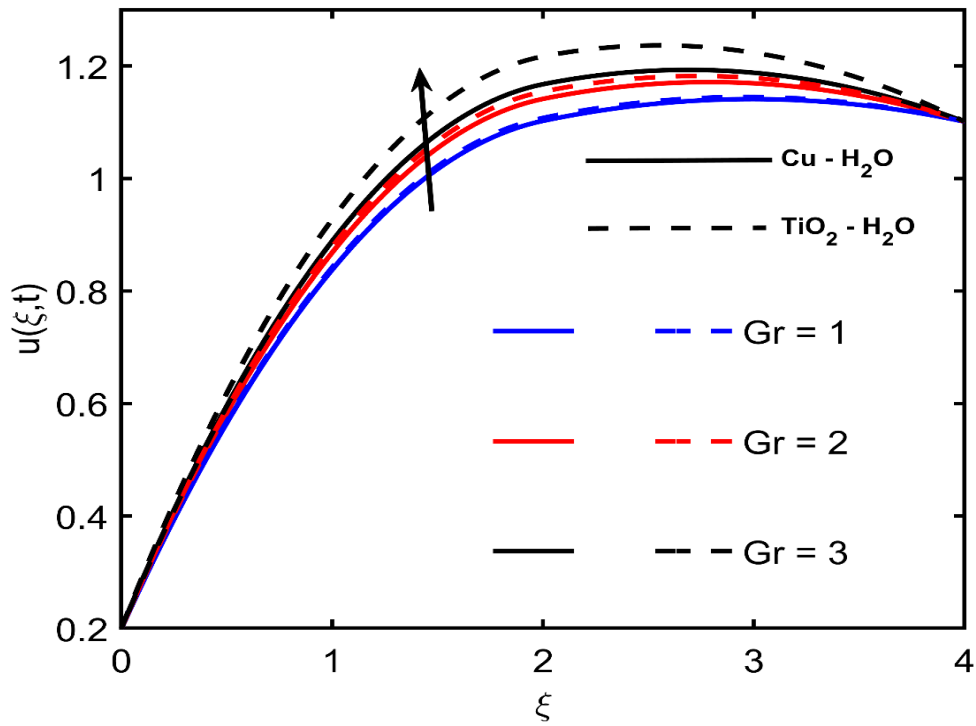


Fig.12: Velocity profiles  $u$  versus  $Gr$ .

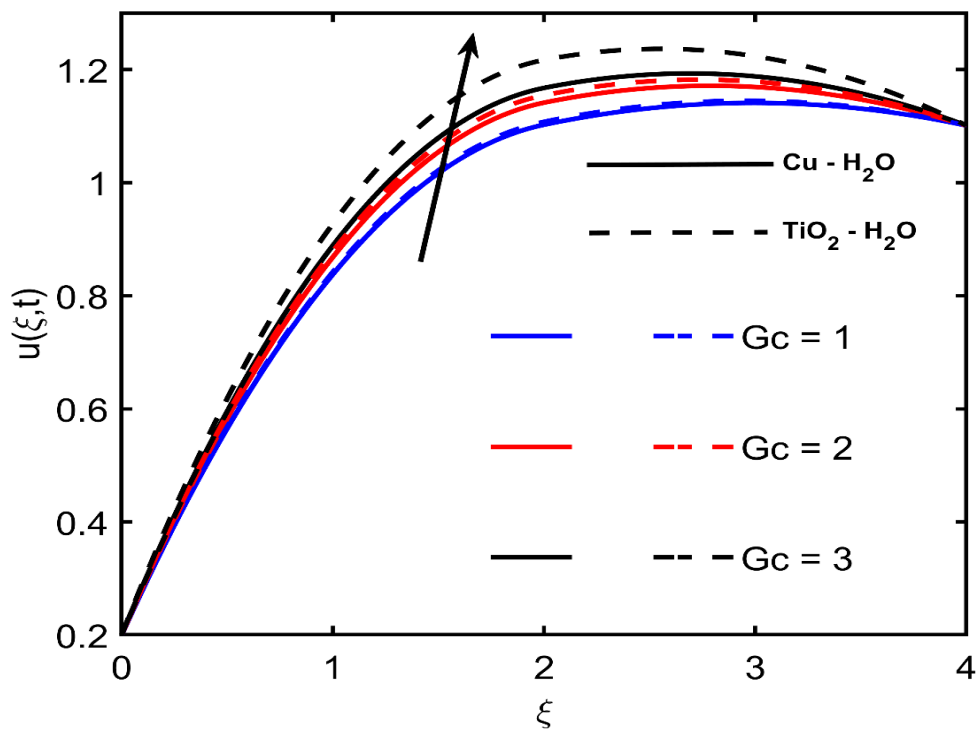


Fig.13: Velocity profiles  $u$  versus  $Gc$ .

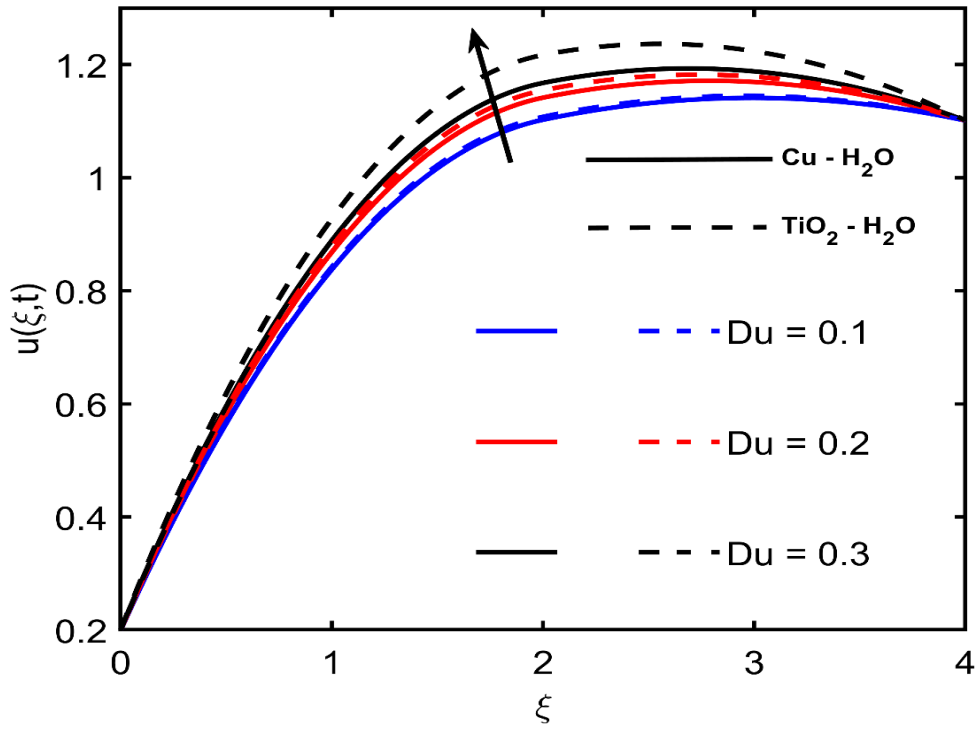


Fig.14: Velocity profiles  $u$  versus  $Du$ .

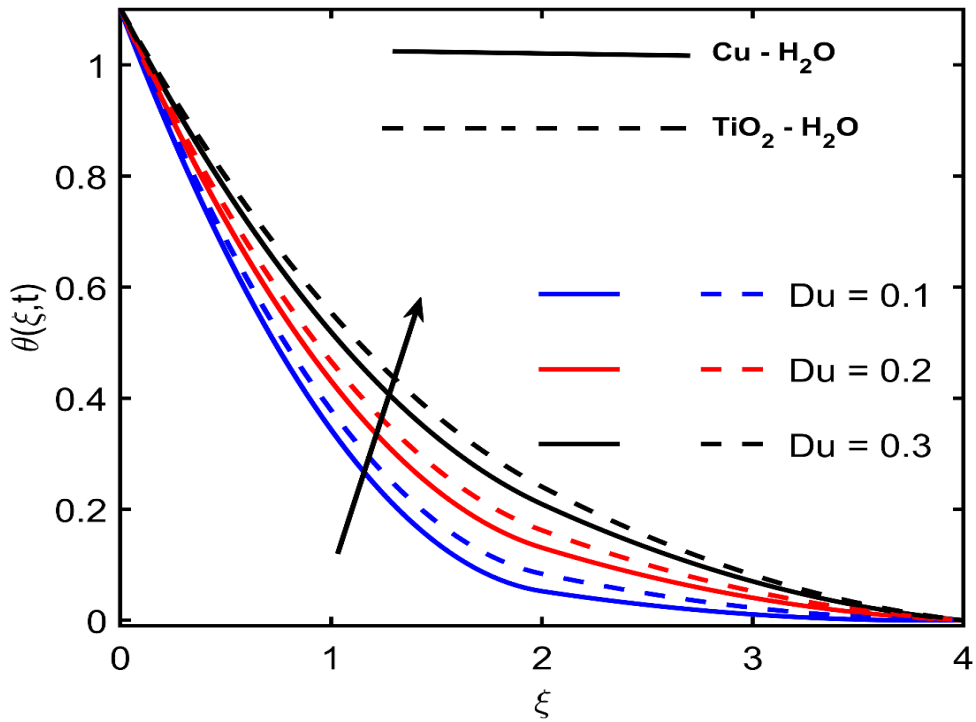


Fig.15: Temperature profiles  $\theta$  versus  $Du$ .

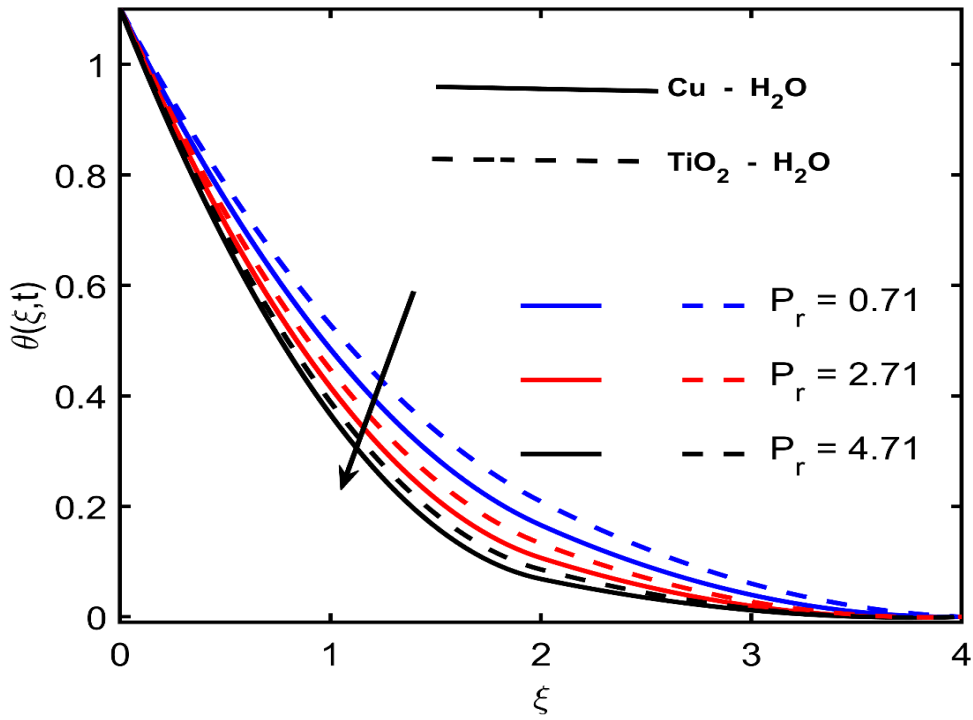


Fig.16: Temperature profiles  $\theta$  versus Pr.

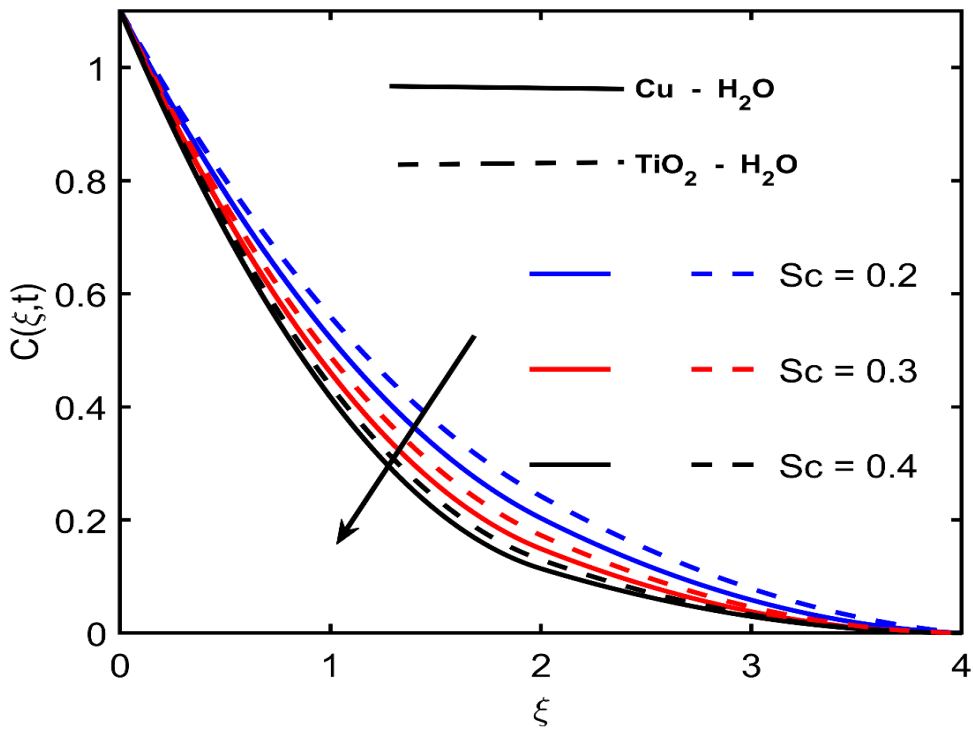


Fig.17: Concentration profiles  $C$  versus Sc.

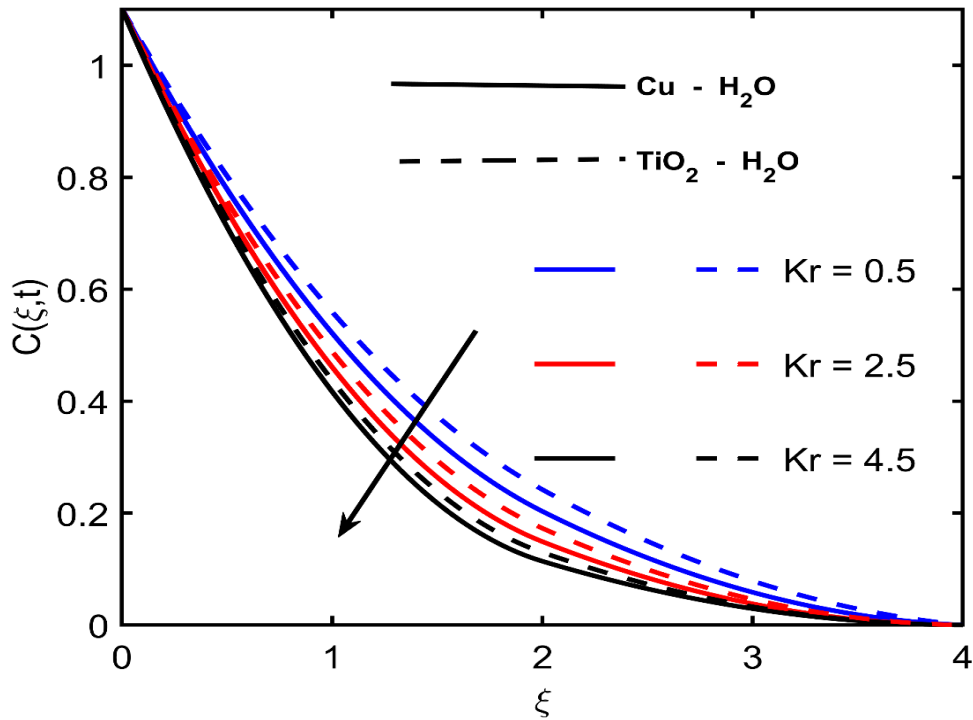


Fig.18: Concentration profiles  $C$  versus  $Kr$ .

The skin friction coefficient ( $S_f$ ) variation for both  $Cu$  - water and  $TiO_2$ -water nanofluids with changes in  $M$ ,  $Gr$ ,  $Gc$ ,  $Du$ ,  $Sr$ ,  $H_s$ , and  $R$  are disclosed in Table 3. It is declared from this table that the skin friction devalues with the increase in  $M$  but it rises with  $Gr$ ,  $Gc$ ,  $Du$ ,  $Sr$ ,  $H_s$ , and  $R$  for both nanofluids. The Nusselt number  $Nu$  variation for

changes in  $Pr$ ,  $N$ ,  $R$ ,  $Du$ , and  $H_s$  are disclosed in Table 4. It is declared from this table that the Nusselt number upsurges with an increment in all the parameters for both nanofluids. The deviation of the Sherwood number  $Sh$  is presented in Table 5 for a variety of  $Sr$ ,  $Sc$ , and  $Ki$ . The Sherwood number grows by expanding  $Sr$  but exhibits a converse trend for  $Sc$  and  $Kr$ .

**Table 3:** Numerical values of the skin friction coefficient.

$M$	$Gr$	$Gc$	$Du$	$Sr$	$H_s$	$R$	$S_f$ for $Cu - H_2O$	$S_f$ for $TiO_2 - H_2O$
0.2	1	1	0.1	0.1	0.1	1	0.39336	0.96383
0.3							0.12110	0.44687
0.4							0.09383	0.39547
	2						0.48711	0.96488
	3						0.57944	0.97238
	4						0.69754	0.99462
		2					0.56364	1.16582
		3					0.63727	1.52599
		4					0.99486	1.69801
			0.4				0.39270	0.96411
			0.5				0.42009	0.98719
			0.6				0.79253	0.99586
				0.4			0.09386	0.39540
				0.5			0.12112	0.44681
				0.6			0.39332	0.96378
					2		0.07861	0.39903
					5		0.11139	0.45042
					6		0.39145	0.96464
						2	0.09383	0.39547
						3	0.12110	0.44687
						4	0.39336	0.96383

Table 4: Numerical variation of  $Nu$ 

Pr	$N$	$R$	$Du$	$H_s$	$Nu$ for $Cu - H_2O$	$Nu$ for $TiO_2 - H_2O$
0.71 6.0 11.62	0.1	0.1	0.1	0.1	0.74886	0.78596
					0.81588	1.00618
					0.98627	1.05019
	0.2	0.3	0.4	0.4	0.78643	0.78978
					0.98499	0.98796
					1.03482	1.03665
	0.4	2	3	4	0.78204	0.78643
					0.97756	0.98304
					1.02644	1.03219
	0.4	0.4	0.5	0.6	0.78645	0.78539
					0.98281	0.98288
					1.03185	1.03340
	0.2	0.3	0.5	0.5	0.78639	0.77442
					0.98108	0.96733
					1.02959	1.01763

Table 5: Numerical variation of  $Sh$ 

$Sc$	$Kr$	$Sr$	$Sh$	
0.22 0.6 0.66	0.5	0.1	0.98638	
			0.94666	
			0.77425	
	1	3	4	0.90850
				0.89744
				0.75686
	0.4	0.5	0.6	0.77562
				0.96956
				1.01812

## CONCLUSION

To enrich the scope and analytical depth of the current study, incorporation of two distinct types of nanofluids was executed:  $TiO_2$ -water and  $Cu$ -water. By employing the Crank-Nicolson implicit method to solve the mathematical model, a thorough investigation of the flow dynamics and heat transfer characteristics of these nanofluids was performed. This robust numerical approach ensured stability and precision in simulating the underlying fluid and thermal phenomena. The key conclusions derived from this analysis are as follows:

- i. The velocity profile for both nanofluids hiked with increments in  $Sr$ ,  $R$ ,  $K_p$ ,  $H_s$ ,  $Gr$ ,  $Gc$ , and  $Du$  while a reverse trend is observed in enhancing  $M$  and  $N$ .
- ii. The fluid temperature exhibited an increase with growing values of  $R$ ,  $H_s$ , and  $Du$  while declined with  $Pr$  and  $N$  values.

- iii. The concentration trend for both fluids upsurged with an increment in  $Sr$  while  $Sc$  and  $Kr$  lessened the concentration.
- iv. The skin friction devalued with the increase in  $M$  but it rose with  $Gr$ ,  $Gc$ ,  $Du$ ,  $Sr$ ,  $H_s$ , and  $R$  for both nanofluids.
- v. The Nusselt number upsurged with an increment  $Pr$ ,  $N$ ,  $R$ ,  $Du$ , and  $H_s$  for both nanofluids.
- vi. The Sherwood number increased on expanding  $Sr$  but exhibited a converse trend for  $Sc$  and  $Kr$ .

## REFERENCES

- H. Babar, H. Wu, W. Zhang, T. R. Shah, D. McCluskey, and C. Zhou, "The promise of nanofluids: A bibliometric journey through advanced heat transfer fluids in heat exchanger tubes," *Advances in Colloid and Interface Science*, vol. 103112, 2024. <https://doi.org/10.1016/j.cis.2024.103112>.

- L. S. Sundar, "Synthesis and characterization of hybrid nanofluids and their usage in different heat exchangers for an improved heat transfer rates: A critical review," *Engineering Science and Technology, an International Journal*, vol. 44, p. 101468, 2023. <https://doi.org/10.1016/j.jestch.2023.101468>.
- M. Mumtaz, S. Islam, H. Ullah, A. Dawar, and Z. Shah, "A numerical approach to radiative ternary nanofluid flow on curved geometry with cross-diffusion and second order velocity slip constraints," *International Journal of Heat and Fluid Flow*, vol. 105, p. 109255, 2024. <https://doi.org/10.1016/j.ijheatfluidflow.2023.109255>.
- J. C. Maxwell, *A Treatise on Electricity and Magnetism*, vol. 1, Oxford: Clarendon Press, 1873.
- S. U. Choi and J. A. Eastman, "Enhancing thermal conductivity of fluids with nanoparticles," Argonne National Lab., Argonne, IL, United States, Rep. No. ANL/MSD/CP-84938; CONF-951135-29, 1995.
- J. Buongiorno et al., "A benchmark study on the thermal conductivity of nanofluids," *Journal of Applied Physics*, vol. 106, no. 9, 2009. <https://doi.org/10.1063/1.3245330>.
- L. Wang and J. Fan, "Nanofluids research: Key issues," *Nanoscale Research Letters*, vol. 5, pp. 1241–1252, 2010. <https://doi.org/10.1007/s11671-010-9656-8>.
- S. S. Murshed and P. Estellé, "A state of the art review on viscosity of nanofluids," *Renewable and Sustainable Energy Reviews*, vol. 76, pp. 1134–1152, 2017. <https://doi.org/10.1016/j.rser.2017.03.113>.
- R. S. Kumar and T. Sharma, "Stability and rheological properties of nanofluids stabilized by SiO<sub>2</sub> nanoparticles and SiO<sub>2</sub>-TiO<sub>2</sub> nanocomposites for oilfield applications," *Colloids and Surfaces A: Physicochemical and Engineering Aspects*, vol. 539, pp. 171–183, 2018. <https://doi.org/10.1016/j.colsurfa.2017.11.056>.
- M. Muneeshwaran, G. Srinivasan, P. Muthukumar, and C. C. Wang, "Role of hybrid-nanofluid in heat transfer enhancement—A review," *International Communications in Heat and Mass Transfer*, vol. 125, p. 105341, 2021.
- T. T. Loong, H. Salleh, A. Khalid, and H. Koten, "Thermal performance evaluation for different type of metal oxide water based nanofluids," *Case Studies in Thermal Engineering*, vol. 27, p. 101288, 2021. <https://doi.org/10.1016/j.csite.2021.101288>.
- S. V. Sujith, H. Kim, and J. Lee, "A review on thermophysical property assessment of metal oxide-based nanofluids: Industrial perspectives," *Metals*, vol. 12, no. 1, p. 165, 2022. <https://doi.org/10.3390/met12010165>.
- H. Yasmin, S. O. Giwa, S. Noor, and M. Sharifpur, "Thermal conductivity enhancement of metal oxide nanofluids: A critical review," *Nanomaterials*, vol. 13, no. 3, p. 597, 2023. <https://doi.org/10.3390/nano13030597>.
- S. M. Hussain, M. R. Mishra, G. S. Seth, and A. J. Chamkha, "Dynamics of heat absorbing and radiative hydromagnetic nanofluids through a stretching surface with chemical reaction and viscous dissipation," *Proceedings of the Institution of Mechanical Engineers, Part E: Journal of Process Mechanical Engineering*, vol. 238, no. 1, pp. 101–111, 2024. <https://doi.org/10.1177/09544089221144077>.
- S. S. Samantaray et al., "Recent advances on entropy analysis of composite nanofluids—A critical review," *Results in Engineering*, p. 101980, 2024. <https://doi.org/10.1016/j.rineng.2023.101980>.
- P. D. Prasad, R. K. Kumar, and S. V. K. Varma, "Heat and mass transfer analysis for the MHD flow of nanofluid with radiation absorption," *Ain Shams Engineering Journal*, vol. 9, no. 4, pp. 801–813, 2018. <https://doi.org/10.1016/j.asej.2017.02.001>.
- U. Ali, M. Y. Malik, A. A. Alderremy, S. Aly, and K. U. Rehman, "A generalized findings on thermal radiation and heat generation/absorption in nanofluid flow regime," *Physica A: Statistical Mechanics and its Applications*, vol. 553, p. 124026, 2020. <https://doi.org/10.1016/j.physa.2020.124026>.
- M. Yaseen et al., "Analysis of heat transfer of mono and hybrid nanofluid flow between two parallel plates in a Darcy porous medium with thermal radiation and heat generation/absorption," *Symmetry*, vol. 14, no. 9, p. 1943, 2022. <https://doi.org/10.3390/sym14091943>.

- T. Thumma et al., "Increasing effects of Coriolis force on the cupric oxide and silver nanoparticles based nanofluid flow when thermal radiation and heat source/sink are significant," *Waves in Random and Complex Media*, pp. 1–18, 2022.  
<https://doi.org/10.1080/17455030.2022.211883>.
- R. Kodi et al., "Hall current and thermal radiation effects of 3D rotating hybrid nanofluid reactive flow via stretched plate with internal heat absorption," *Results in Physics*, vol. 53, p. 106915, 2023.  
<https://doi.org/10.1016/j.rinp.2023.106915>.
- C. Sulochana, G. P. Ashwinkumar, and N. Sandeep, "Effect of frictional heating on mixed convection flow of chemically reacting radiative Casson nanofluid over an inclined porous plate," *Alexandria Engineering Journal*, vol. 57, no. 4, pp. 2573–2584, 2018.  
<https://doi.org/10.1016/j.aej.2017.08.011>.
- B. K. Sharma, U. Khanduri, N. K. Mishra, and K. S. Mekheimer, "Combined effect of thermophoresis and Brownian motion on MHD mixed convective flow over an inclined stretching surface with radiation and chemical reaction," *International Journal of Modern Physics B*, vol. 37, no. 10, p. 2350095, 2023.  
<https://doi.org/10.1142/S0217979223500952>.
- N. Vijay and K. Sharma, "Entropy generation analysis in MHD hybrid nanofluid flow: Effect of thermal radiation and chemical reaction," *Numerical Heat Transfer, Part B: Fundamentals*, vol. 84, no. 1, pp. 66–82, 2023.  
<https://doi.org/10.1080/10407790.2023.2174204>.
- D. Sunil, D. Garg, V. K. Joshi, K. Sharma, and S. Kumar, "Effect of thermal radiation on Bodewadt flow in the presence of porous medium," *Pramana*, vol. 97, no. 1, p. 16, 2023.  
<https://doi.org/10.1007/s12043-022-02467-1>.
- R. Bordoloi, D. Gohain, N. Ahmed, and A. J. Chamkha, "An exact analysis of radiation absorption and Dufour effect on MHD convective flow of Cu-water nanofluid with heat generation and chemical reaction," *International Communications in Heat and Mass Transfer*, vol. 127, p. 105592, 2021.  
<https://doi.org/10.1016/j.icheatmasstransfer.2021.105592>.
- M. D. Shamshuddin, F. Shahzad, W. Jamshed, O. A. Bég, M. R. Eid, and T. A. Bég, "Thermo-solutal stratification and chemical reaction effects on radiative magnetized nanofluid flow along an exponentially stretching sensor plate: Computational analysis," *Journal of Magnetism and Magnetic Materials*, vol. 565, p. 170286, 2023.  
<https://doi.org/10.1016/j.jmmm.2022.170286>.
- M. D. Shamshuddin and K. K. Asogwa, "Non-Newtonian Casson Nanoliquid Flowing through Device: Physical Impact of Heat Producing and Radiation," *Mathematical Modelling of Fluid Dynamics and Nanofluids*, vol. 322, 2023.
- N. K. Reddy, H. K. Swamy, M. Sankar, and A. Yoon, "Impact of internal heat generation/absorption on MHD conjugate flow of aqueous-MWCNT nanofluid in a porous annulus," *Journal of Thermal Analysis and Calorimetry*, pp. 1–15, 2023.  
<https://doi.org/10.1007/s10973-023-12112-x>.
- H. Upreti, A. K. Pandey, N. Joshi, and O. D. Makinde, "Thermodynamics and heat transfer analysis of magnetized Casson hybrid nanofluid flow via a Riga plate with thermal radiation," *Journal of Computational Biophysics and Chemistry*, vol. 22, no. 3, pp. 321–334, 2023.  
<https://doi.org/10.1142/S2737416523500216>.
- V. Puneeth, R. Anandika, S. Manjunatha, and O. D. Makinde, "Quadratic convection on the radiative flow of ternary nanofluid Gr–Ag–TiO<sub>2</sub>–H<sub>2</sub>O subjected to velocity slip and temperature jump," *International Journal of Modern Physics B*, vol. 38, no. 9, p. 2450125, 2024.  
<https://doi.org/10.1142/S021797922450125X>.
- H. Sardar, L. Ahmad, M. Khan, and A. S. Alshomrani, "Investigation of mixed convection flow of Carreau nanofluid over a wedge in the presence of Soret and Dufour effects," *International Journal of Heat and Mass Transfer*, vol. 137, pp. 809–822, 2019.  
<https://doi.org/10.1016/j.ijheatmasstransfer.2019.03.109>.
- V. B. Bekezhanova and O. N. Goncharova, "Influence of the Dufour and Soret effects on the characteristics of evaporating liquid flows," *International Journal of Heat and Mass Transfer*, vol. 154, p. 119696, 2020.

- M. Jawad, A. Saeed, P. Kumam, Z. Shah, and A. Khan, "Analysis of boundary layer MHD Darcy-Forchheimer radiative nanofluid flow with Soret and Dufour effects by means of Marangoni convection," *Case Studies in Thermal Engineering*, vol. 23, p. 100792, 2021.  
<https://doi.org/10.1016/j.csite.2020.100792>.
- N. Shaheen, H. M. Alshehri, M. Ramzan, Z. Shah, and P. Kumam, "Soret and Dufour effects on a Casson nanofluid flow past a deformable cylinder with variable characteristics and Arrhenius activation energy," *Scientific Reports*, vol. 11, no. 1, p. 19282, 2021.  
<https://doi.org/10.1038/s41598-021-98516-3>.
- I. Siddique, M. Nadeem, J. Awrejcewicz, and W. Pawłowski, "Soret and Dufour effects on unsteady MHD second-grade nanofluid flow across an exponentially stretching surface," *Scientific Reports*, vol. 12, no. 1, p. 11811, 2022.  
<https://doi.org/10.1038/s41598-022-15985-4>.
- B. P. Reddy, O. D. Makinde, and A. Hugo, "A computational study on diffusion-thermo and rotation effects on heat generated mixed convection flow of MHD Casson fluid past an oscillating porous plate," *International Communications in Heat and Mass Transfer*, vol. 138, p. 106389, 2022.  
<https://doi.org/10.1016/j.icheatmasstransfer.2022.106389>.
- M. D. Shamshuddin, S. Panda, A. Saeed, P. K. Ratha, and S. R. Mishra, "Homotopy analysis on magnetized Williamson-micropolar nanofluid flow over a bi-directionally extending surface with multiple slip conditions," *Numerical Heat Transfer, Part B: Fundamentals*, pp. 1–21, 2024.  
<https://doi.org/10.1080/10407790.2023.2250810>.
- N. Vijay and K. Sharma, "Magnetohydrodynamic hybrid nanofluid flow over a decelerating rotating disk with Soret and Dufour effects," *Multidiscipline Modeling in Materials and Structures*, vol. 19, no. 2, pp. 253–276, 2023.  
<https://doi.org/10.1108/MMMS-11-2022-0301>.
- N. K. Mishra, M. Sharma, B. K. Sharma, and U. Khanduri, "Soret and Dufour effects on MHD nanofluid flow of blood through a stenosed artery with variable viscosity," *International Journal of Modern Physics B*, vol. 37, no. 30, p. 2350266, 2023.  
<https://doi.org/10.1142/S0217979223502663>.
- K. A. Duguma, O. D. Makinde, and L. G. Enyadene, "Stability analysis of dual solutions of convective flow of Casson nanofluid past a shrinking/stretching slippery sheet with thermophoresis and Brownian motion in porous media," *Journal of Mathematics*, vol. 2023, no. 1, p. 5954860, 2023.  
<https://doi.org/10.1155/2023/5954860>.
- R. Sharma, "Transient MHD Free Convection Flow, Heat and Mass Transfer in Darcy–Forchheimer Porous Medium in the Presence of Chemical Reaction and Heat Absorption with Soret and Dufour Effects: Element-Free Galerkin Modelling," *Mathematical Models and Computer Simulations*, vol. 15, no. 2, pp. 357–372, 2023.  
<https://doi.org/10.1134/S2070048223020152>.
- M. B. Patil, K. C. Shobha, S. Bhattacharyya, and Z. Said, "Soret and Dufour effects in the flow of Casson nanofluid in a vertical channel with thermal radiation: entropy analysis," *Journal of Thermal Analysis and Calorimetry*, vol. 148, no. 7, pp. 2857–2867, 2023.  
<https://doi.org/10.1007/s10973-022-11630-3>.
- F. Shah, T. Hayat, and S. Momani, "Non-similar analysis of the Cattaneo-Christov model in MHD second-grade nanofluid flow with Soret and Dufour effects," *International Journal of Thermal Sciences*, vol. 135, pp. 145–154, 2019.  
<https://doi.org/10.1016/j.ijthermalsci.2018.09.028>.
- G. C. Mishra, R. S. R. Gorla, and R. K. Agarwal, "Soret and Dufour effects on MHD heat and mass transfer in non-Darcy porous medium," *Journal of Heat Transfer*, vol. 140, no. 7, p. 072001, 2018.  
<https://doi.org/10.1115/1.4038467>.

F. Mabood, N. K. Shukla, and Z. Abbas, "Impact of thermophoresis and Brownian motion on MHD radiative Casson nanofluid flow with Dufour and Soret effects," Alexandria Engineering Journal, vol. 57, no. 2, pp. 1411–1421, 2018.  
<https://doi.org/10.1016/j.aej.2017.03.048>.

M. Hamid, S. Hossain, and Z. Abbas, "Impact of Thermophoresis and Brownian Motion in Three-Dimensional Hydromagnetic Flow of Casson Nanofluid with Joule Heating and Nonlinear Thermal Radiation," IEEE Access, vol. 7, pp. 142680–142691, 2019.  
<https://doi.org/10.1109/ACCESS.2019.2944370>.